ACS APPLIED POLYMER MATERIALS

pubs.acs.org/acsapm

Article

# Electrochemical and Nanostructural Characterization of Poly(3,4-ethylenedioxythiophene):poly(styrenesulfonate) Films as Coatings for Neural Electrodes

Yuanmin Zhang, Yuqi Chen, Sonia Contera,* and Richard G. Compton*

Cite This: *ACS Appl. Polym. Mater.* 2023, 5, 5555−5566

Read Online

ACCESS | Metrics & More | Article Recommendations | Supporting Information

**ABSTRACT:** Poly(3,4-ethylenedioxythiophene) (PEDOT), a well-characterized conducting polymer, has been applied for coating metal neural electrodes to improve their stimulating or recording performance. The coated electrodes possess advantages in better neuron attachment, lower impedance, and larger capacitance compared to the bare metal substrate due to the biocompatibility and porous surface of the polymer. However, the PEDOT-coated electrodes have frequently reported issues associated with mechanical instability, such as cracking and delamination. Solving this problem is crucial for stimulating electrodes, whereas a massive film is unnecessary for recording purposes. Moreover, the thickness control for the latter has rarely been investigated. In this work, we systematically studied and characterized poly(3,4-ethylenedioxythiophene):poly(styrenesulfonate) (PEDOT:PSS) with cyclic voltammetry and atomic force microscopy (AFM) to evaluate the electropolymerization of PEDOT:PSS from the basis and analyze the surface morphology for a range of deposition times. The polymerization potential was obtained, and the deposition charge density was optimized for recording neural electrodes. In addition, high-resolution AFM height and phase images reveal the heterogeneity of the polymer surface. The modified electrode was also tested for its electrochemical performance in a small potential window with both a standard electrochemical cell setup and stainless steel microscrews. The results showed that despite a shift of potential (0.42 V) due to the change of setup, the electrode functions well in the capacitive region without triggering redox reactions.

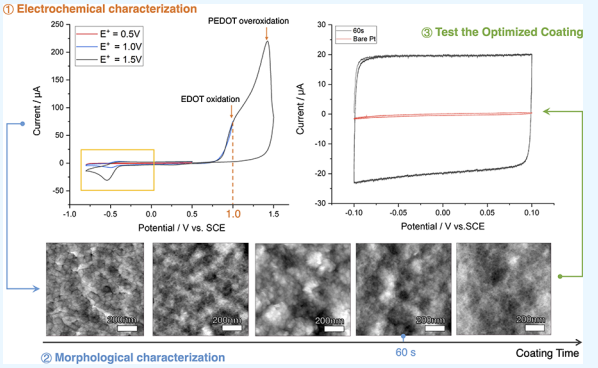


**KEYWORDS:** *PEDOT:PSS, electrochemical analysis, surface morphology, CV, AFM, neural electrodes*



## 1. INTRODUCTION

Implantable neural devices are widely exploited in neuroscience research to probe electrically active cells.[1] However, due to their microscopic size and interfacial rigidity, many metal electrodes suffer from high impedance as well as being susceptible to surface fouling, thereby limiting the signal-to-noise ratio and restricting the lifetime of implanted electrodes.[1] Since the development of conducting polymers (CPs) in the last century, broad attention has been given to electrode coatings on the surface of the electrodes to reduce these problems and to enhance the performance of neural electrodes. The layer of a CP on the metallic or silicon substrate substantially reduces the impedance as the roughened, porous surface produces a larger electrochemical surface area.[2] The soft polymer layer also separates the hard substrate surface from the tissue, mitigating the immune response, and there have even been reports of preferential in vitro and in vivo neuron growth.[3] Thanks to their superior conductivity, chemical stability,[4] and biocompatibility, CPs have the potential to elevate the performance of traditional neural electrodes to new levels.

Poly(3,4-ethylenedioxythiophene) (PEDOT) is one of the most promising candidates for CP-modified neural electrodes. PEDOT possesses good conductivity[4,5] and has been shown in vitro to promote cell adhesion and exhibit low cytotoxicity[6] and little immune response following electrode insertion in vivo,[7] which is crucial for long-term in vivo recording. The common ways of PEDOT deposition include spin coating[8] and electropolymerization. However, for electrodes such as tetrodes, it is challenging to carry out spin coating, as cross-linking between the different recording sites can easily arise. Electropolymerization is a better and more controllable approach where the fabrication process can be tailored by tuning the polymerization conditions (potential/current,

Received: April 24, 2023
Accepted: June 3, 2023
Published: June 21, 2023

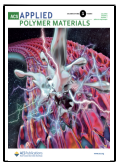

**Table 1. Summary of PEDOT:PSS Electropolymerization Methods**

| material[a] | substrate[b] | method | voltage applied[c] | current applied | deposition time | ref |
|---|---|---|---|---|---|---|
| PEDOT:PSS | Au | galvanostatic | | 0.5−2.0 mA $cm^{-2}$ | charge deposition from 133−1667 mC $cm^{-2}$ | 9 |
| | | potentiostatic | 1.1 V (vs SCE) | | | |
| PEDOT:PSS | Pt | galvanostatic | | 0.64 mA $cm^{-2}$ | 10−500 s | 5 |
| PEDOT:PSS | Pt | galvanostatic | | 0.2 mA $cm^{-2}$ | 71−1071 s | 26 |
| PEDOT:PSS | Pt, ITO | potentiostatic | 0.0 → 0.5 V for 10 s, 0.75 → 1.4 V for 110 s (vs SCE) | | 120 s | 14 |
| PEDOT:PSS | Au | CV | 5−25 mV $s^{-1}$, 0.9−1.2 V (vs SCE) | | | 20 |
| | | potentiostatic | 0.8, 0.9, 1.1 V (vs SCE) | | 10−50 s | |
| | | galvanostatic | | 0.03−0.5 mA $cm^{-2}$ | 10−900 s | |
| PEDOT:PSS | glassy carbon, Au | potentiostatic | 1 V (vs AglAgCl) | | charge limited to 260 mC $cm^{-2}$ | 27 |
| PEDOT:PSS | Pt | galvanostatic | | 0.5 mA $cm^{-2}$ | 100−2000 s | 6 |
| PEDOT:$ClO_4$ | Pt | galvanostatic | | 0.5 mA $cm^{-2}$ | 33 min 20 s | 11 |
| PEDOT:BS | | | | | | |
| PEDOT:PTS | | | | | | |
| PEDOT:DBS | | | | | | |
| PEDOT:PSS | | | | | | |
| PEDOT:TEAP | Ir | galvanostatic | | 0.5 mA $cm^{-2}$ | charge deposition from 50−1000 mC $cm^{-2}$ | 10, 28 |
| PEDOT:$BF_4$ | PtIr | galvanostatic | | | limit charge to 260 mC $cm^{-2}$ | 12 |
| PEDOT:PSS + MWCNT | Pt | galvanostatic | | 0.02 mA $cm^{-2}$ | 50−400 s | 29 |
| | | potentiostatic | 1 V (vs AglAgCl) | | 50−400 s | |
| PEDOT:PSS + MWCNT | Pt/Ir | potentiostatic | 1.3 V (vs AglAgCl) | | 30 s | 30 |

[a]PEDOT:poly(3,4-ethylenedioxythiophene). PSS: polystyrene sulfonate. TEAP: tetraethylammonium perchlorate. $ClO_4^-$: perchlorate. BS: benzenesulfonate. pTS: *p*-toluenesulfonate. DBS: dodecylbenzene sulfonate. $BF_4^-$: tetrafluoroborate. MWCNT: multi-walled carbon nanotube. [b]Au: gold. Pt: platinum. ITO: indium tin oxide. Ir: iridium. Pt/Ir: platinum/iridium alloy. [c]SCE: saturated calomel electrode. AglAgCl: silver chloride electrode.

polymerization charge density, and dopant). Table 1 summarizes several PEDOT electropolymerization methods.

Cui and Martin[9] reported one of the earliest attempts at electrochemically depositing PEDOT onto a metal electrode for neuronal recordings. The coated electrode exhibited better electrical properties in terms of impedance and charge storage capacities compared to the bare electrodes. Their work focused on coating, particularly with stimulating electrodes,[5] demonstrating that there is a charge injection limit with increasing thickness of the coating and that a thicker film is always accompanied by mechanical failure such as cracking and delamination. For recording electrode arrays, Ludwig et al.[10] showed that compared to uncoated sites, those coated with PEDOT provided higher quality recording in terms of better signal-to-noise ratio and a greater number of viable units registered. Moreover, they also found that the impedance decreased with increasing deposition but was limited for deposition charges larger than 260 mC $cm^{-2}$.

The mechanism of electropolymerization of PEDOT has been studied. The reaction scheme is shown in Supporting Information Scheme S1. Applying current or potential to the working electrode initiates the formation of the radical cation of the PEDOT monomer, leading to the growth of the polymer film possibly via radical−radical dimerization followed by further electrochemical oxidation, which with further addition of monomeric units forms oligomeric chains. The ultimate polymer chain is a combination of oligomeric and monomer radicals, with positive charges spread along the backbone. The charge requires the polymerization to be accompanied by the uptake of anions from the solution. Anions that have been used include perchlorate ($ClO_4^-$), benzenesulfonate (BS), *p*-toluenesulfonate (pTS), dodecylbenzene sulfonate (DBS), and tetrafluoroborate ($BF_4^-$), leading to different bulk properties,[11,12] but the use of polystyrene sulfonate (PSS) is common as is evident from Table 1 partly due to the easy processability of the films[13] and partly since the synthesis is claimed to be green.[13] The transition of the growing polymer from the molecular to the macroscopic scale has been explored by Tamburri et al.[14] who discussed the growth mechanism of PEDOT in terms of polymer nucleation with the subsequent 3D growth blanketing the entire surface. Note that at high potentials, $PEDOT^+$ can undergo further oxidation, but the resultant products are complicated and have been covered by other literature studies.[15−17] Such overoxidation is likely to lead to irreversible chemical changes with a negative impact on essential properties, notably conductivity.[14,15]

PEDOT:PSS is attractive for biological applications because of its mixed ion−electron conductivity which is useful in converting biological signals (ionic motion) into electrical signals (electronic motion).[18] The mixed conduction emerges from the two-phase nature of the material, where PEDOT-rich regions are embedded with PSS-rich regions.[13] The hydration of PSS is thought to encourage ion transport within the structure, and the aggregated PEDOT regions are responsible for hole transport.[8,13,19] PEDOT-rich and PSS-rich regions are interconnected, which implies that the whole bulk is involved in the charge interaction, giving rise to a volumetric capacitance. Furthermore, PEDOT:PSS possesses a relatively high specific capacitance originating from the large effective double-layer area due to its porous surface.[8,13,19] The capacity is thus closely related to material morphology.

The morphology reflects several factors, such as the polymerization method used, the solvent, and the choice of dopant. Castagnola et al.[20] investigated the effect of different



https://doi.org/10.1021/acsapm.3c00861
ACS Appl. Polym. Mater. 2023, 5, 5555−5566

electropolymerization routes, where potential scanning approaches created the most homogeneous surface. However, very few researchers use this approach due to the uncontrollable current.[21] A range of dopants[11] and solvents[12] were also studied to address the issues of chemical and mechanical stabilities.

While it has been established that PEDOT-modified electrodes demonstrate a lower impedance than bare electrodes (especially at low frequency, <100 kHz[5]), the main ongoing challenge relates to the mechanical stability of the film which is closely related to the film thickness. This is a particular problem for stimulating electrodes rather than recording electrodes, where in the former case, thicker films are used to improve the charge injection capacity so that the injected charge is large enough to trigger neural membrane depolarization. On the other hand, a thick film is unnecessary for a recording electrode, in particular, where little outperformance can be gained over the impedance. In addition, previous research has reported delamination and cracking problems associated with a thick coat and reduced biocompatibility.[5,6,21,22] For a film with charge deposition larger than 0.5 C $cm^{-2}$, PEDOT-coated electrodes showed no advantage over bare Pt in terms of biological benefits.[6] There is so far very little research about film thickness reported in the literature for recording electrodes. Other methods, notably incorporation of PEDOT:PSS hydrogel,[23] to maintain film integrity are useful for macro sensor fabrication but not easy for microwire metal electrodes, especially those with closely packed detection spots (e.g., as in the tetrodes often used in vivo) where the hydrogel easily overgrows and cross-connects different detection points. Thickness control is an obvious gap in the published research and is an effective way to control and improve the mechanical stability of the film for recording electrodes.

In vivo experiments often report a reduction in signal with time partly due to the fact that the metal microwire presents a rigid non-biocompatible interface contacting the tissue that causes immune responses which may result in the formation of an encapsulating layer called a glial scar isolating the electrode from the neurons.[24] Therefore, the purpose of the present work is to coat the metal interface with a soft conducting polymer to make the surface biocompatible. Generally, little or no effort has hitherto been made in respect over control of the thickness of the CP layer formed on the recording electrodes. In addition, as a volumetric capacitor, the morphological change post-implantation is crucial but has not been investigated.

In this work, the electrodeposition of PEDOT:PSS is systematically studied and characterized with cyclic voltammetry (CV) and atomic force microscopy (AFM) from the perspective of use for neural electrodes in the recording mode. Surface morphology is studied as a function of the conditions of deposition. The roughness of the surface is quantified; surface nanoscale heterogeneity is revealed and discussed. The surface morphology is assessed as a function of exposure to aqueous media in the form of deionized water and phosphate-buffered solution (PBS) with the latter being a suitable medium for short-term in vitro characterization.[25] Electrochemical measurements, both Faradaic and capacitive, are investigated both with a well-defined reference electrode [a saturated calomel electrode (SCE)] and with a stainless steel (SS) microscrew pseudo-reference electrode mirroring the typical approach adopted for in vivo experiments (in rodents) where both such screws act as both reference and counter electrodes. Measurements under the two approaches were seen to be equivalent except for a shift of potential of 0.42 V, allowing the electrochemical data found under rigorous electrochemical conditions to be applied to inform in vivo experiments. Our optimized coating (as assessed via morphological and electrochemical analyses) suggests a charge deposition of ca. 50 mC $cm^{-2}$, which showed better biological[6] and electrical responses compared to naked Pt electrodes. The data collected therefore provides an essential basis for the use of PEDOT:PSS as a coating for neural metal electrodes particularly when used in the recording mode.

## 2. MATERIALS AND METHODS

**2.1. Materials.** 3,4-Ethylenedioxythiophene (EDOT, 97% purity), poly(sodium 4-styrenesulfonate) (NaPSS, average $M_w$ = 70,000), and PBS were purchased from Sigma-Aldrich and used as received. Deionized water with a resistivity of 18.2 MΩ cm at 298 K (Millipore, Millipak Express 20, Watford, UK) was used.

A Pt macro disk (area = 0.02 $cm^2$) and a Pt single crystal (Miller indices (100) and active area ≈ 0.22 $cm^2$) were used as working electrodes to perform electrochemical characterization and morphological studies.

**2.2. Electropolymerization.** Experiments were carried out in a thermostated Faraday cage using a μ-AutolabIII potentiostat/galvanostat (Autolab B.V., Utrecht, The Netherlands) with NOVA software. A standard three-electrode setup was employed with Pt as the working electrode, a SCE (BSi Inc., West Lafayette, IN, USA) as the reference electrode, and a graphite rod as the counter electrode. All working electrodes were washed with deionized water and dried with nitrogen prior to electropolymerization. The Pt macro disk was polished on soft lapping pads with alumina powder of decreasing size (1.0, 0.3, and 0.05 μm; Buehler IL, UK) each time before each experiment. The Pt single-crystal electrode was cleaned by heating to red heat using a Bunsen burner for 10 s to remove surface impurities.

The electropolymerization was conducted potentiostatically in a solution containing 10 mM EDOT and 0.1 mM NaPSS [0.7% (w/v)].[14,20] Constant potentials with values between 0.5 and 1.5 V were applied for 0.5−120 s. The cell solution was kept at 25 ± 1 °C and degassed with nitrogen for 10 min before each electrochemical experiment.

**2.3. Electrochemical Characterization.** All the electrochemical characterizations were carried out in a three-electrode cell setup with either a SCE as the reference electrode and a graphite rod as the counter electrode or, to mimic the in vivo setup, stainless steel microscrews (SS, M1.4) as the reference and counter electrodes. Electrodes were immersed in polymerization solution (10 mM EDOT and 0.1 mM NaPSS) or 0.1 mM NaPSS solution for investigation via CV with a wide potential scanned between 0.5 and 1.7 V and at a scan rate of 50 mV $s^{-1}$. Small potential window scans from −100 to 100 mV with scan rates 25, 50, 100, and 200 mV $s^{-1}$ in 0.01 M PBS were undertaken to test electrode functioning in the range of neuronal activity.

To obtain the reference potential shift between the SCE/graphite setup and the SS/SS setup, both wide scans (−0.8 to 2.0 V) and small scans (−100 to 100 mV) were carried out separately with these two setups, immersing a modified Pt electrode (about 50 mC charge deposition) in 0.01 M PBS solution.

**2.4. Atomic Force Microscopy.** The polymer film morphology was analyzed by Cypher atomic force microscopy (Cypher AFM, Asylum Research, Oxford Instrument, CA, USA). Olympus AC240TSA cantilevers ($f_{resonance}$ ≈ 70 kHz, $k_c$ ≈ 2.0 N $m^{-1}$) were used to probe the surface. Images of topography and phase were acquired by tapping mode in deionized water or 0.01 M PBS and were collected and processed by Igor Pro software (Oxford Instruments Asylum Research). The cantilever was calibrated by the Sader method[31] and tuned before any test, so the phase was 90° when the cantilever was not in contact with the sample. During the tapping, the



https://doi.org/10.1021/acsapm.3c00861
ACS Appl. Polym. Mater. 2023, 5, 5555−5566

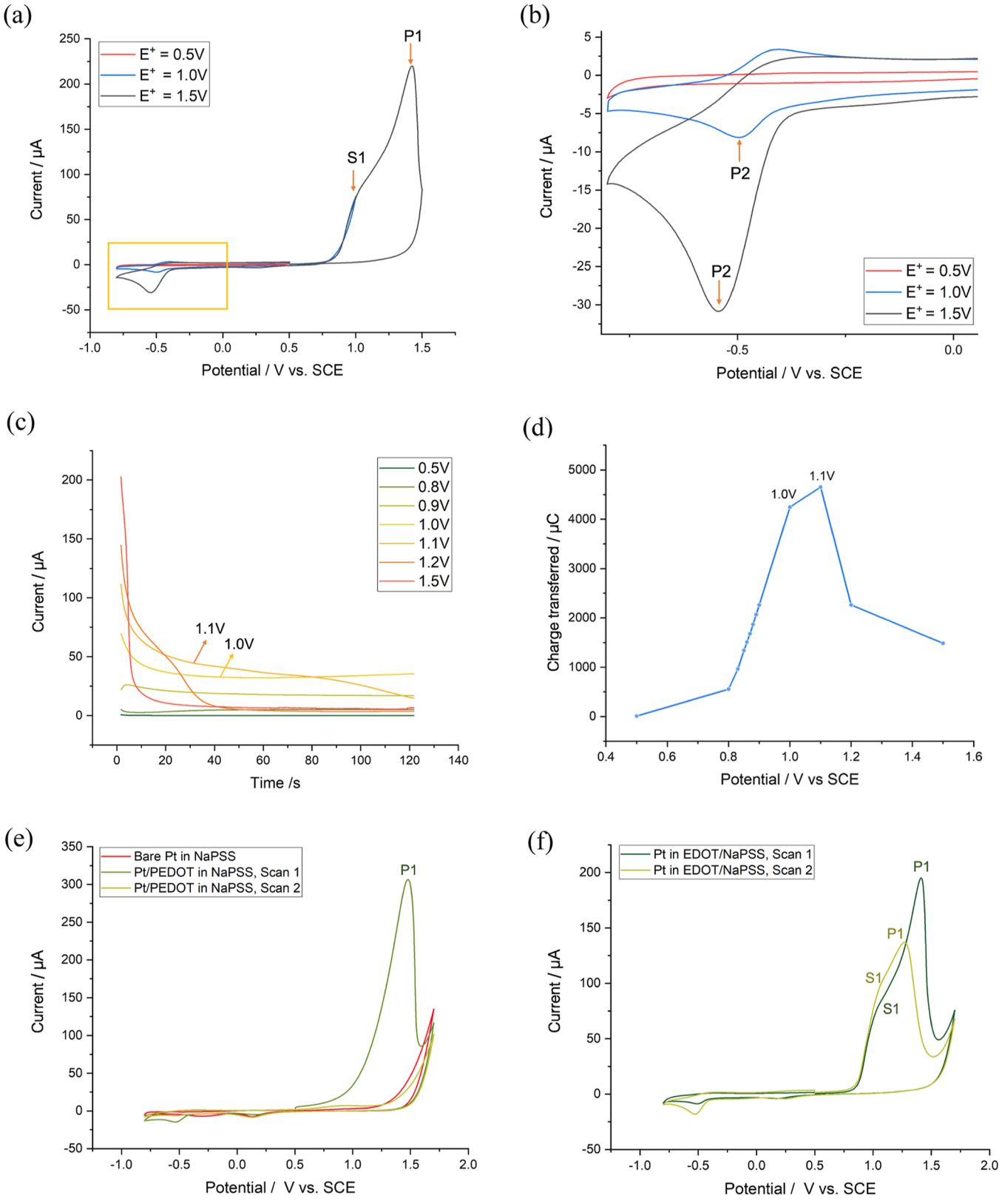


**Figure 1.** (a,b) CV of a bare Pt disc electrode immersed in 10 mM EDOT and 0.1 mM NaPSS solution. The scan started at 0.5 V, swept anodically up to different limits ($E^+$ = 0.5 V, 1.0 V, and 1.5 V vs SCE), then reverse-scanned to a fixed cathodic limit at −0.8 V, and eventually returned to 0.5 V (0.5 V → $E^+$ → −0.8 V → 0.5 V vs SCE). The yellow box for (a) is enlarged and shown in (b). (c) Chronoamperograms using the same electrode and solutions were recorded at potentials between 0.5 and 1.5 V vs SCE. (d) Variation of the amount of charge transferred during electropolymerization in (c) with potential 0.5−1.5 V vs SCE. (e) Comparison of the CV scans of the modified Pt (green and yellow) and bare Pt (red) disc electrodes in 0.1 mM NaPSS (0.5 V → 1.7 V → −0.8 V → 0.5 V vs SCE). (f) CV scans of a Pt disc electrode in 10 mM EDOT and 0.1 mM NaPSS (0.5 V → 1.7 V → −0.8 V → 0.5 V vs SCE).



https://doi.org/10.1021/acsapm.3c00861
ACS Appl. Polym. Mater. 2023, 5, 5555−5566

**Scheme 1. Procedures for Morphological Characterization. DW: Deionized Water. PBS: Phosphate-Buffered Saline**

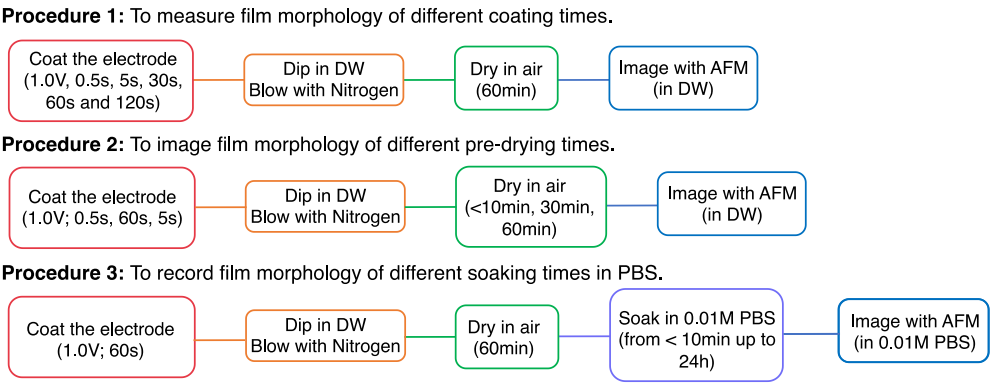


atomic force microscope operates in a small amplitude range (<10 nm).[32] The root-mean-square (RMS) roughness of each full image was calculated by the following equation

$$R_{rms} = \sqrt{\frac{1}{N}\sum Y_i^2}$$

where $R_{rms}$ is the RMS roughness, $N$ is the number of data points, and $Y$ is the height value of each data point.[33]

## 3. RESULTS AND DISCUSSION

In this section, we first discuss the electrochemical properties of EDOT to determine the optimum coating potential. Subsequently, the selected voltage was applied to investigate the potentiostatic mode of coating for different deposition times and thus optimize the process. The film morphology, roughness, and stability were then investigated utilizing AFM in the tapping mode. Finally, with the deposition potential and time optimized, the final modified electrode was tested in 0.01 M PBS as a good medium for short-term in vitro electrochemical characterization.[25]

**3.1. Electrochemical Characterization of EDOT.** First, the electrochemical properties of EDOT in an aqueous solution were analyzed using CV. Initial CV scans started at a potential of 0.50 V (vs SCE), swept anodically to 1.5 V, then swept cathodically to −0.80 V, and eventually returned to 0.50 V using a bare disc Pt electrode immersed in 10 mM EDOT and 0.1 mM NaPSS solution (Figure 1a,b). The choice of 0.5 V as the initial potential is to ensure that no Faradaic reaction happens until the scan has reached higher potentials than the start potential. Otherwise, the resulting voltammogram would be distorted. For the anodic scan, a peak (P1) can be observed at around 1.4 V (vs SCE), together with a shoulder (S1) in the proximity of 1.0 V. On the cathodic scan, a reduction peak P2 is seen with a peak potential of −0.55 V. The magnitude of this peak is much smaller than that of the oxidation peak P1. To understand S1 and evaluate its nature, we recorded further CV scans in which the maximum anodic potentials ($E^+$) were 0.50 and 1.0 V, keeping the cathodic limit the same as before. The resultant CV scans are compared and shown in Figure 1a,b. The red line ($E^+$ = 0.5 V) has neither a reduction peak (P2) at −0.55 V nor a small oxidation peak at −0.42 V, implying no PEDOT formation at its maximum potential. For the reduction peak (P2) to be seen in the reverse scan, a threshold potential of ca. 1.0 V in the anodic scan is required. The presence of the reduction peak confirms that there was Faradaic oxidation at S1.

Comparison with the literature[14] suggests that S1 corresponds to monomer oxidation and hence to the onset of polymerization.

Next, potential step chronoamperometry was applied to a solution of identical composition as used for CV, with the value of the applied potential of the Pt electrode jumping from 0 V (vs SCE) to a fixed value ranging from 0.5 to 1.5 V (Figure 1c). The total charge passed in the chronoamperograms up to a time of 120 s was calculated and summarized (Figure 1d). At low potentials, little current and hence charge was seen or passed in the chronoamperograms. After the onset of monomer oxidation around and near 1.0 V (vs SCE), currents flow nearly steadily, with increasing charge and current seen for increasing potentials up to 1.0 V. Above this potential, the initially steady current dies away after prolonged electrolysis as is apparent in the current−time curve measured for a potential step to 1.1 V. This loss of electroactivity is especially apparent in Figure 1d where for potentials more anodic than 1.1 V, the charge passed drops markedly. It is likely that for potentials of 1.1 V or more, there is overoxidation of the polymer film, leading to irreversible chemical changes[14,15] in addition to consumption of a monomer.

To investigate this hypothesis further, the Pt electrode was coated in the potentiostatic mode at 1.0 V for 120 s, transferred to a 0.1 mM NaPSS solution, and CV scanned (0.5 V → 1.7 V → −0.8 V → 0.5 V vs SCE). The result is shown in Figure 1e and compared with the same scan in a solution with the presence of 10 mM EDOT (Figure 1f). The former shows that the application of potential larger than 1.1 V to a preformed film completely destroyed the oxidative electroactivity. Therefore, after the first scan, the CV of the subsequent scan had little difference from a scan with a bare Pt in NaPSS. It is evident that the sustained application of an oxidizing potential in excess of ca. 1.0 V to the film causes overoxidation and loss of voltammetric signal likely due to the loss of film conductivity as observed by others.[15]

It was concluded that for potentiostatic deposition, the optimum potential was +1.0 V (vs SCE) and that potentials in excess of this value caused an irreversible chemical change to the film. Next, we investigated the impact of the length of time of the deposition.

**3.2. Morphological Characterization of EDOT.** To optimize the coating time, an initial series of films were produced on a Pt single crystal (100) of size 0.22 $cm^2$ compatible with the atomic force microscope used for imaging the surfaces and for measuring their roughness. The procedures are illustrated in Scheme 1. In general, a



https://doi.org/10.1021/acsapm.3c00861
ACS Appl. Polym. Mater. 2023, 5, 5555−5566

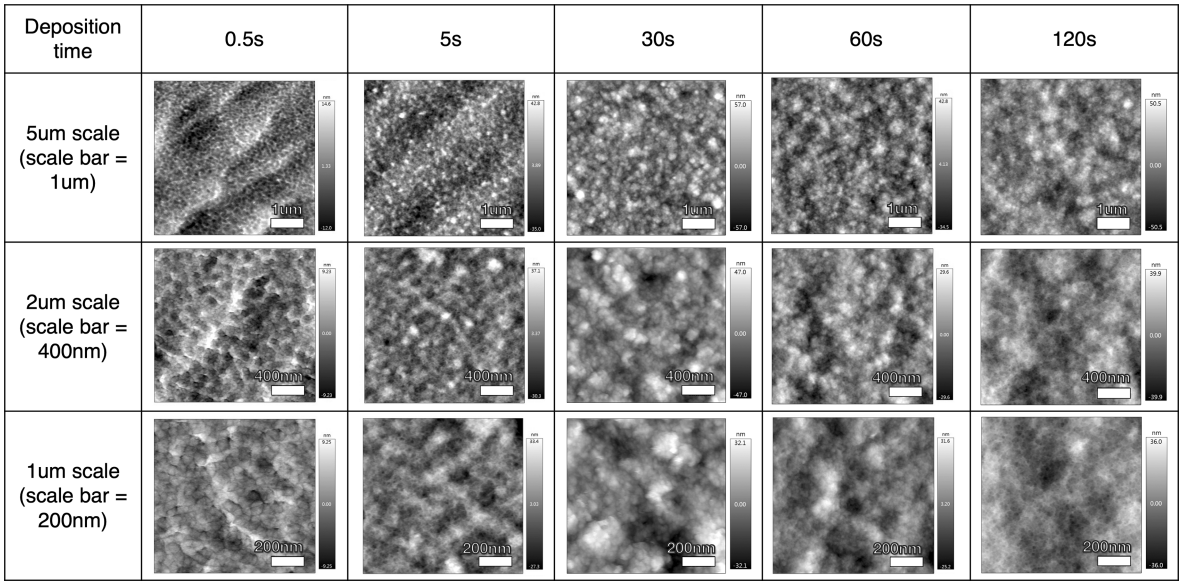


**Figure 2.** Morphology of PEDOT:PSS-coated Pt electrode surfaces obtained by tapping mode AFM in deionized water. Deposition times range from 0.5 to 120 s, and the images are magnified to different scales (5, 2, and 1 $\mu$m scan frames). The scale bars for the panel are 1 $\mu$m, 400 nm, and 200 nm from the top to the bottom row, respectively.

potentiostatic deposition of PEDOT was performed on a Pt single crystal at 1 V for a range of times depending on the particular test. After the coating, the electrode was dipped in deionized water, blown with nitrogen to remove excess liquid, and then left at room temperature for an hour or less depending on the exact experiments of interest before further testing. Note that beyond the coatings indicated in Scheme 1, thicker films have been made using a Pt macro disk electrode, but the surface was found to be mechanically fragile and, notably, easily cracked, for example, by simply blowing dry nitrogen over the surface (Supporting Information Figure S1). No such behavior was inferred for the coverage developed on our thinner layer-coated electrodes. Film morphologies were observed in an aqueous environment formed from either a few drops of deionized water or PBS placed on the film before imaging using the AFM tapping mode.

Note that all of the final imaging steps were carried out in aqueous conditions (deionized water or PBS). Performing the imaging in liquid provided several advantages, notably giving higher resolution compared to those obtained in the air, where the resolution was compromised at a small scale because a water moisture layer on the polymer surface makes the interaction potential between the tip and the sample more complex, decreasing the resolution[34] (Supporting Information Figure S2a). In addition, in the in vivo environment, the ion species responsible for interaction are primarily provided by extracellular fluid (ECF), where a 0.01 M PBS can be useful as a short-term in vitro substitution for electrochemical and nanostructural characterization.[25] From the polymer deposition characterization point of view, the disadvantage of imaging in liquid was that the polymer would inevitably swell to a larger size than in air. To minimize such effects, we performed AFM imaging as fast as possible (within 30 min) after adding the liquid drop to the dried polymer. In addition, drying in the air before imaging also helps to better observe the small features. From Supporting Information Figure S2b, the polymers were in circular shape (ca. 50 nm) until a drying time of 60 min where a finely meshed and porous structure (Supporting Information Figure S2c) similar to natural cotton balls (Supporting Information Figure S2d) could be observed.

For procedures 1 and 2 (Scheme 1), the polymer was imaged in deionized water instead of PBS due to the much faster rate of swelling of the film in PBS. Given the same pre-drying time in the air (60 min) and a similar soaking time in solution (<10 min), the film roughness was larger in PBS than in deionized water (Supporting Information Figure S3). More direct visual evidence of swelling is shown in Supporting Information Figures S4i and S5d, which indicate that the polymer swells into circular bulbs (ca. 50 nm) in PBS but that a finely meshed and porous structure was visible in deionized water. The images in PBS are thought to be close to those expected for ECF. Procedure 3 was applied to keep track of polymer swelling in 0.01 M PBS from less than 10 min up to a prolonged period of 24 h. The final imaging was conducted in the same solution as the soaking solution to prevent disturbing the surface from changing the solution. The swelling of the film in PBS will reach equilibrium, which will be discussed in Section 3.2.3.

Overall, in the context of the metal electrode for a neuronal recording application environment, swelling of the pre-dried films following fabrication takes place. However, performing imaging in deionized water after a pre-drying period produced enhanced resolution and detail in the surface features, and imaging in 0.01 M PBS provided a satisfactory environment for transient studies. These approaches and initial observations gave a basis for recording the more detailed data given in the following sections.

*3.2.1. Film Morphology of Different Coating Times.* For the results reported in this section, procedure 1 (Scheme 1) was followed. Figure 2 summarizes the images for various coating times and at different magnification scales.

The images of the 0.5 s coating surface in Figure 2 reveal the very initial stages of polymer growth on a Pt substrate for the first time at high resolution (from 5 × 5 $\mu$m to 1 × 1 $\mu$m scan frames). The short-time deposition sample consisted of circular segments growing next to each other, enclosing a


https://doi.org/10.1021/acsapm.3c00861
ACS Appl. Polym. Mater. 2023, 5, 5555−5566

pore in the middle with an average depth of 6 nm (Supporting Information Figure S6). The presence of pores could lead to the exposure of the underlying Pt surface. For the 5 s deposition sample, small granules (bright dots) can be observed, and they are connected by a finely meshed network. These grains are inferred to be growing polymer nuclei, PEDOT, embedded in the PSS matrix, as proposed previously.[13,14] From the images, it can be observed that a large number of nuclei (ca. 15 ± 2 per $\mu m^2$) form within the first 5 s of growth (see high-contrast image, Supporting Information Figure S7) in contrast to observations using indium tin oxide[14] (ca. 4 ± 2 per $\mu m^2$) as the substrate where much fewer nuclei were observed, indicating possible benefits of using platinum electrodes for reproducible and more homogeneous films. These nuclei grew in size as the deposition proceeded and the average film thickness (Table 2, estimated

**Table 2. Summary of Average Charge-Transferred Density during Chronoamperometry and Estimation of Average Film Thickness on the Pt Electrode**

| coating time (s) | average charge-transferred density (mC $cm^{-2}$) | estimation of average thickness[a] (nm) |
|---|---|---|
| 0.500 ± 0.001 | 0.49 ± 0.04 | 3.2 ± 0.3 |
| 5.000 ± 0.001 | 4.6 ± 0.4 | 30 ± 3 |
| 30.000 ± 0.001 | 22 ± 2 | 150 ± 10 |
| 60.000 ± 0.001 | 47 ± 4 | 310 ± 30 |
| 120.000 ± 0.001 | 87 ± 7 | 570 ± 50 |

[a]Assume the total volume of the polymer deposited evenly across the electrode substrate.

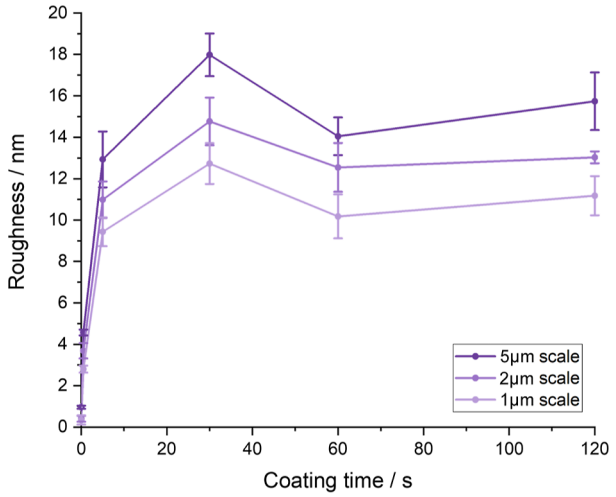


**Figure 3.** RMS roughness of the PEDOT:PSS surfaces in Figure 2. The *y*-intercepts (coating time = 0 s) are the RMS roughness of the bare Pt electrodes. The error bars represent the surface roughness variation in three different spots on the film.

from the amount of charge transferred) increased. Figure 3 records the variation of surface RMS roughness with deposition time; the initial roughness is only about 1 nm larger than the bare substrate, indicating a relatively flat surface for 0.5 s coating. For a deposition time of 5 s or above, the surface roughness reached a steady value.

To assess the coating coverage, the phase images of films formed by 0.5 and 5 s coatings were recorded as shown in Figure 4. The phase images contain information of the topography as well as the energy dissipation at the interface. The contrast in the phase signals gives insights into different types of materials over which the cantilever is being scanned, where a hard surface usually produces a higher phase signal compared to softer areas, and is related to the energy dissipated at the interface.[13,32,35] A significant contrast between different areas was obtained in the 0.5 s coating (Figure 4a), in which the labeled points correspond to the peaks of phase along the measurement line across the surface. The corresponding positions relate to the pores in the height image, suggesting that the Pt surface may be partially exposed at these sites. In the phase diagram recorded for the 5 s coating, although the line passes through several dark and bright regions (Figure 4b), their phase has little difference without any dominant peaks observed as in the 0.5 s image. The phase variation, in this case, is attributed to scanning through the PSS-rich and PEDOT-rich regions.[13]

It has been reported that PEDOT:PSS cast onto a glass substrate[13] is a two-phase material consisting of PEDOT-rich and PSS-rich grains, where a PEDOT-rich grain is about 10−20 nm in size and the PSS-rich grain is about 20−30 nm.[13,36] The single grain size is similar to the phase variation period (16 nm, evaluated by averaging the peak separation) along the drawn line imposed in Figure 4b. Further zooming into the 5 s deposition image gives Figure 4c,d, from which one can observe that the bright regions in the height image (e.g., box A) are dark in the phase image and vice versa (e.g., box B). The inhomogeneous polymer surface is shown schematically in Figure 4e. When the polymer is immersed in an aqueous environment, the PEDOT-dominant zones (box B) are expected to be relatively hydrophobic in comparison to the PSS-dominated parts, which are thought to take up water and hence are expected to swell and soften. The swelled polymer leads to higher height signals, but the soft areas are assigned to the dark-phase signals. A rough estimation from Figure 4c suggests that the order of magnitude of a PEDOT-dominant region is about 70 nm, and the PSS-dominant region is about 80 nm, which means every one of these regions consists of several PEDOT, PSS-rich grains.

*3.2.2. Film Morphology Resulting from Different Pre-drying Times.* In this section, Procedure 2 (Scheme 1) was followed for the preparation of samples for imaging.

The aim was to inspect the change of surface morphology over the drying time as it could provide information on how long time after coating should the neuronal probe be used biomedically and also to test the variation of surface roughness due to drying. The AFM images are shown in Supporting Information Figure S4, and the roughness is reported in Figure 5a. The polymer swelling over a short time of drying (<60 min) was significant as the mesh-like structure disappeared and was replaced by circular bulbs on the surface (Supporting Information Figure S4). As a result of swelling, all the films exhibited increasing roughness with decreasing drying times in the air (Figure 5a). The roughness of the films formed by 5 and 60 s of electrodeposition was similar throughout the drying time, but the 60 s film has its roughness variation within 1 nm for all scales. Moreover, polymers were prone to adhere to the cantilever tip producing blurred images for a short drying period (Supporting Information Figure S4a,e). Therefore, to have a film securely attached to the electrode, a long enough drying time needs to be allowed before any tests are made that might potentially rupture the surface.



https://doi.org/10.1021/acsapm.3c00861
ACS Appl. Polym. Mater. 2023, 5, 5555−5566

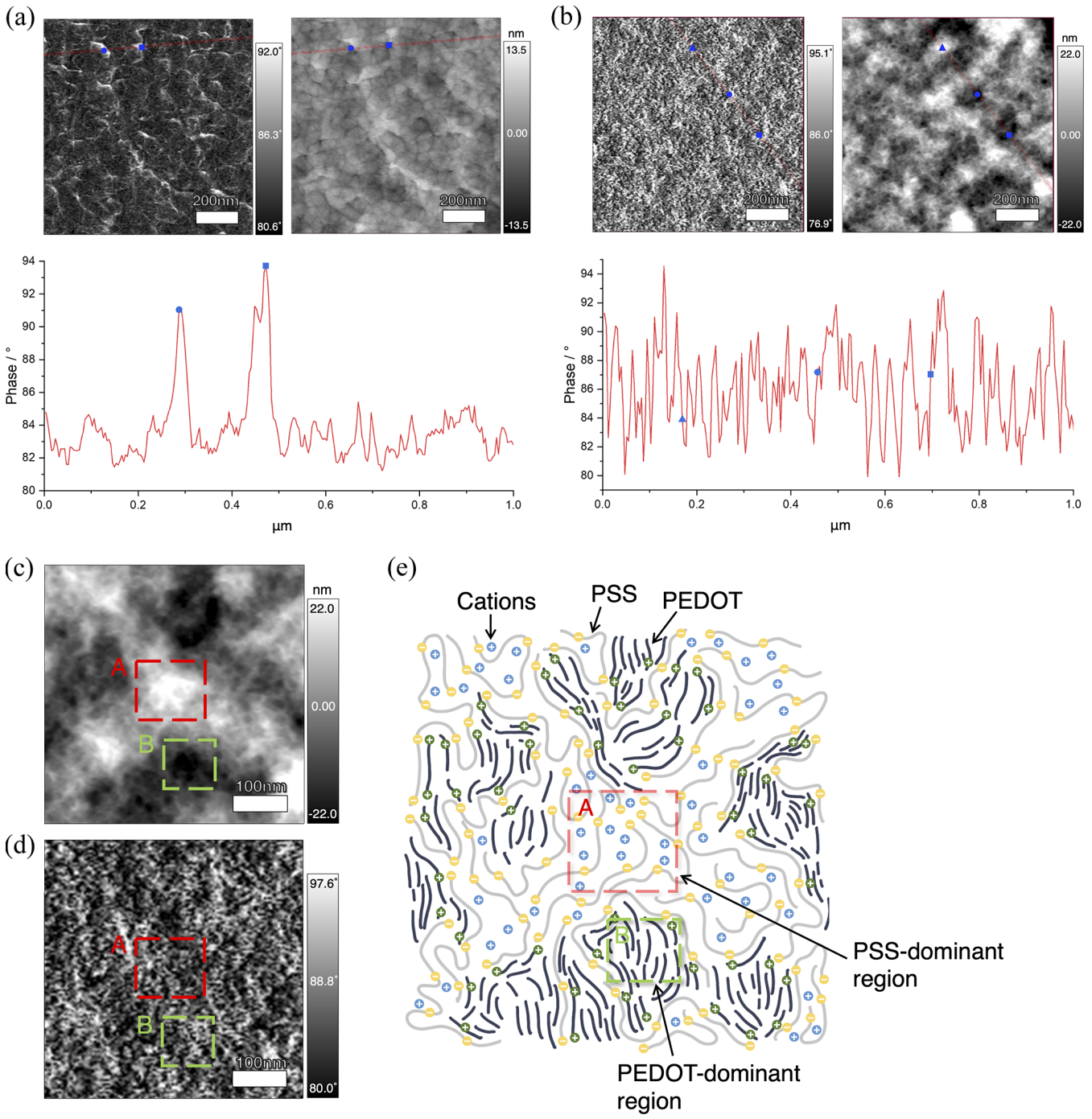


**Figure 4.** (a,b) For both (a) and (b), top left: AFM phase image in deionized water; top right: AFM height image in deionized water. These two graphs are of the same area, and the scale bars all represent 200 nm. A red line is drawn to reveal the phase variation across the surface, and the result is shown in the bottom graph. (a) 0.5 s coating and dried in air for 1 h. Two positions, corresponding to the peaks in phase data, are labeled by a circle and a square, respectively. The positions in the height image coincide with the position of the pores. (b) 5 s coating and dried in air for 1 h. The red line passes through several bright and dark regions in the height image, but there is little contrast in the phase diagram (For height data along the line please, see Supporting Information Figure S8). (c,d) Height and phase AFM images in deionized water: zoom in on the 5 s deposition surface. Scale bars: 100 nm. (e) Schematic generalization of the inhomogeneous distribution of material on the surface. Adapted with permission from ref 13 (Copyright 2017, John Wiley and Sons). Gray line and yellow charge: $PSS^-$ chain and the excess charges on the chain. Dark line and green charge: $PEDOT^+$ polymer and its charge. Blue charge: cations in the solution. Box A: PSS-dominant region. Box B: PEDOT-dominant region.

*3.2.3. Film Morphology of Different Soaking Times in PBS.* In this section, procedure 3 (Scheme 1) was followed for the preparation of samples for imaging.

The aim is to conduct a short-term in vitro characterization within an ionic solution, 0.01 M PBS functions as an appropriate medium. A 60 s coating time was selected as it is the point where its roughness had reached its plateau value (Figure 3 after 5 s) and had the least roughness variation with different drying times (Figure 5a).



https://doi.org/10.1021/acsapm.3c00861
ACS Appl. Polym. Mater. 2023, 5, 5555−5566

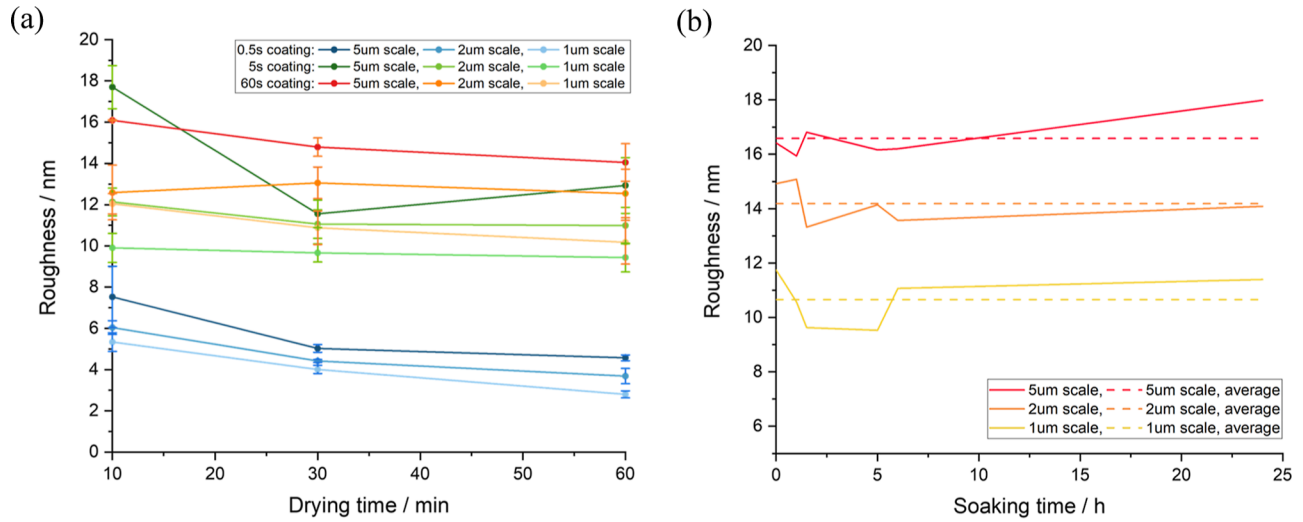


**Figure 5.** (a) Change of RMS roughness of different thickness PEDOT:PSS surfaces as dried in air. (b) 60 s coating, change in RMS roughness for a range of soaking times in 0.01 M PBS.

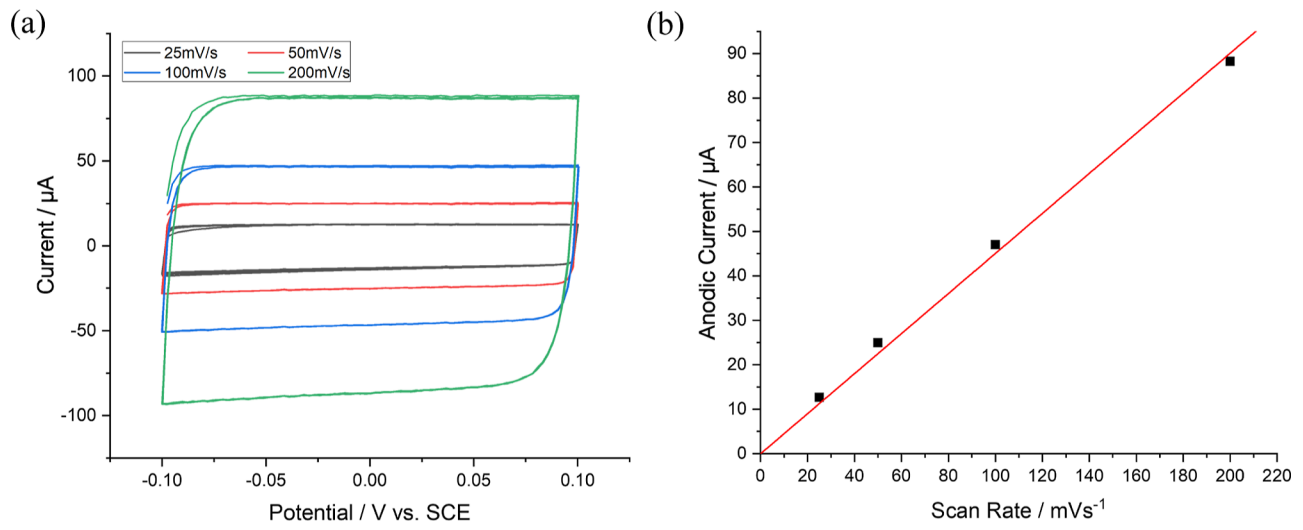


**Figure 6.** (a) CV of a Pt electrode formed by potentiostatic electrodeposition for 60 s immersed in 0.01 M PBS. The scan started at −0.10 V, swept anodically up to 0.10 V, and reverse-scanned to −0.01 V. The scan continued for a total of five cycles for each scan rate. (b) The anodic current in (a) measured at 0 V is plotted against the scan rate. The result is a straight line through the origin (slope = 0.450 ± 0.010 $\mu$F and $R^2$ = 0.99858).

From the AFM images (Supporting Information Figure S5), the faster swelling rate compared to deionized water turned the polymer quickly into spherical shapes when put into PBS for less than 10 min. The trend in Figure 5b suggests that with the prolonged soaking time, the polymer swelling will reach equilibrium as the roughness value (solid line) fluctuates around its average (dash line) for all scales throughout the soaking time. The results are expected as PBS contains a greater number of ions than deionized water, increasing the rate of cation uptake, and the leveling off of the roughness indicates a maximum extent of swelling where the polymer stops absorbing cations and water. The reproducibility of the film was also tested by drying a freshly coated film overnight and soaking it in PBS for 4 h. The roughness obtained was close to the same average value illustrated in Figure 5b across all the scales (Supporting Information Figure S9).

**3.3. Electrochemical Test on a Modified Electrode.** The previous section reported tests on electrodes coated with PEDOT:PSS and fabricated via potentiostatic electrodeposition at 1.0 V for a range of times (0.5−120 s). A preferred coating time of 60 s was established. To further test the performance of electrodes fabricated in this manner, a narrow CV scan was carried out to obtain capacitive data relevant to the recordings made when monitoring in vivo neuronal activity where the detected potential is usually tiny and within the range of −1.5 and +1.5 mV.[37,38]

To ensure complete coverage of the full range of likely potentials to be encountered in vivo, a CV scan was carried out between −100 and + 100 mV versus SCE and tested with various scan rates of 25, 50, 100, and 200 mV $s^{-1}$ for continuous five cycles. The resulting voltammograms are shown in Figure 6a, revealing capacitive behavior within this potential window with a nearly rectangle-shaped cyclic voltammogram without any discernible redox peaks. The five repeated scans in each case overlay well, indicating little variation on the electrode coating surface during the scan. The anodic currents were measured at 0 V versus SCE corresponding to the steady-state plateau in Figure 6a and plotted against the scan rate. The result shown in Figure 6b, which displays a direct proportionality between the current and



https://doi.org/10.1021/acsapm.3c00861
ACS Appl. Polym. Mater. 2023, 5, 5555−5566

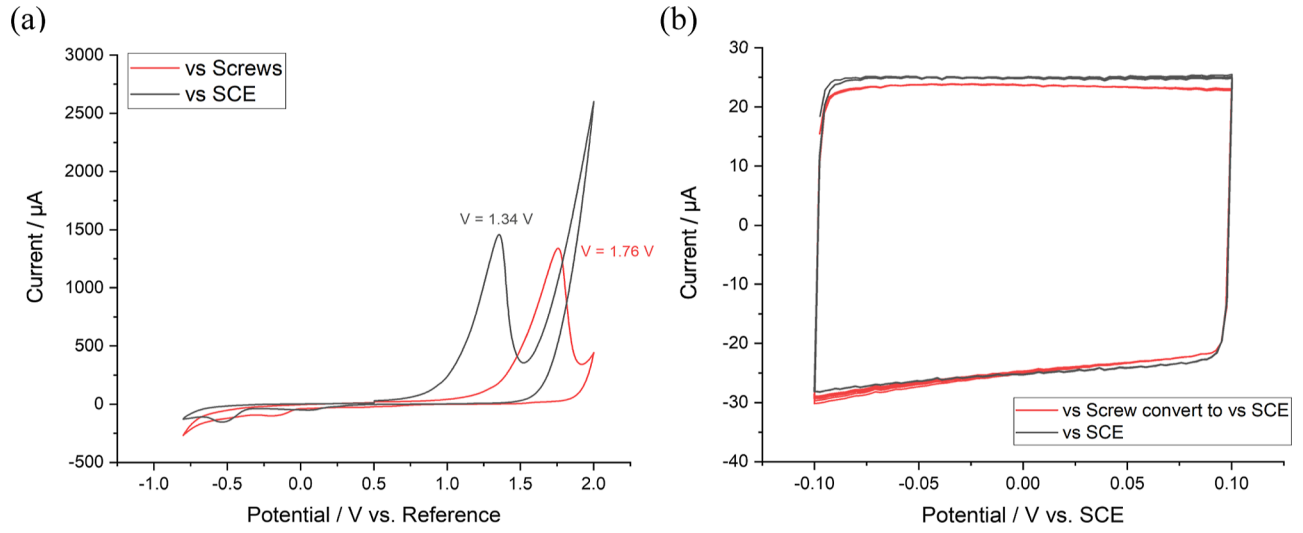


**Figure 7.** (a) CV scan of the 60 s-coated Pt electrode immersed in 0.01 M PBS solution. The scan started at 0.50 V and swept anodically up to 2.0 V, then reverse-scanned to a cathodic limit at −0.80 V, and eventually returned to 0.50 V (0.50 V → 2.0 V→ −0.80 V → 0.50 V). A shift in the peak potential to anodic potentials can be observed, and the shift is $\Delta V = 0.42 \pm 0.01$ V. (b) Small window CV scan of the 60 s-coated Pt electrode immersed in 0.01 M PBS solution. The recorded potential vs SS setup was converted to vs SCE by subtracting $\Delta V$ found in (a). Black line: standard electrochemical cell setup with graphite rod and SCE as the ground and reference electrodes, respectively. Red line: in vivo experimental setup with stainless steel microscrews (SS) as the ground and reference electrodes.

scan rate, is consistent with a pure capacitive behavior of the modified electrode within the small potential window. The fitted straight line passes the origin with a slope of 0.450 ± 0.010 $\mu$F and $R^2$ = 0.999. From the gradient of the linear line, the specific capacitance can be obtained (2.0 ± 0.2 mF cm$^{-2}$). The significantly large value of the capacitance compared to that of the bare electrode surface (Supporting Information Figure S10, ca. 80-folder larger) implies a large electrochemical surface area introduced by the porous structure polymer coated on the surface.

For many in vivo experiments, the electrode setup differs from a standard electrochemical cell setup. Stainless steel (SS) microscrews are commonly used as both reference and ground (counter) electrodes.[39] To compare the potentials measured using a SS microscrew as a pseudo-reference electrode with that of a SCE, a wide scan (0.50 V → 2.0 V→ −0.80 V → 0.50 V) was scanned with a 60 s-coated electrode immersed in 0.01 M PBS, respectively, using the graphite rod/SCE setup and SS/SS setups. A broad scan range was chosen to ensure the coverage of the oxidation peak of PEDOT to facilitate the identification of the difference in reference potential compared to the SCE. Figure 7a shows a noticeable shift in the peak to more anodic values after changing the standard cell setup to the SS/SS setup. The shift in oxidation potential ($\Delta V$) was 0.42 ± 0.01 V corresponding to the difference in the reference potential of the SS compared to the SCE. Cyclic voltammograms corresponding to Figure 6a were also made using the SS/SS setup and converted to the SCE scale, as shown in Figure 7b, demonstrating a satisfactory overlay.

## 4. CONCLUSIONS

The systematic electrochemistry and morphological studies reveal an optimum potential of 1 V for the electrodeposition of PEDOT:PSS, and the subsequent surface roughness/morphology evaluation suggested 60 s as a preferable coating time corresponding to a charge deposition of ca. 50 mC cm$^{-2}$, which represents a balance between depositing sufficient polymer to ensure that no part of the underlying electrode surface is exposed while maintaining the bulk and thickness of the coating in the interests of mechanical stability. Importantly, the high-resolution AFM images provide clear evidence of an inhomogeneous distribution of the PEDOT and PSS grains across the surface with an average size of ca. 16 nm. Last, measurements in both Faradaic and capacitive regions of the voltammetry with saturated calomel reference and stainless steel pseudo-reference electrodes show that reliable electrochemistry can be performed under in vitro conditions in which stainless steel electrodes are used as both (pseudo-)reference and counter electrodes. The potential shift between the two electrodes is 0.42 V. Importantly, the electrode performance in the capacitive region is unaffected. Therefore, the neural electrode can function without triggering redox reactions, altering the surface chemistry with the use of a pseudo-reference electrode despite the usual reservations. The use of neural electrodes is anticipated for in vivo studies based on the coatings of PEDOT:PSS, especially in the recording mode and to which our future attention will be directed.

## ■ ASSOCIATED CONTENT

### Supporting Information

The Supporting Information is available free of charge at https://pubs.acs.org/doi/10.1021/acsapm.3c00861.

AFM images of PEDOT in air, in PBS, and after different pre-drying times before imaging in deionized water; AFM height and phase image data; RMS roughness comparison in deionized water and in PBS; reproducibility of the film RMS roughness after swelling; CV scans of coated and bare Pt electrodes; and image of the cracked PEDOT thick film (PDF)

## ■ AUTHOR INFORMATION

### Corresponding Authors

**Sonia Contera** − *Clarendon Laboratory, Department of Physics, University of Oxford, Oxford OX1 3PU, Great*



https://doi.org/10.1021/acsapm.3c00861
ACS Appl. Polym. Mater. 2023, 5, 5555−5566

*Britain;* orcid.org/0000-0002-2371-1206; Email: sonia.antoranzcontera@physics.ox.ac.uk

**Richard G. Compton** − *Physical and Theoretical Chemistry Laboratory, Department of Chemistry, University of Oxford, Oxford OX1 3PU, Great Britain;* orcid.org/0000-0001-9841-5041; Email: richard.compton@chem.ox.ac.uk

### Authors

**Yuanmin Zhang** − *Clarendon Laboratory, Department of Physics, University of Oxford, Oxford OX1 3PU, Great Britain; Physical and Theoretical Chemistry Laboratory, Department of Chemistry, University of Oxford, Oxford OX1 3PU, Great Britain*

**Yuqi Chen** − *Physical and Theoretical Chemistry Laboratory, Department of Chemistry, University of Oxford, Oxford OX1 3PU, Great Britain*

Complete contact information is available at: https://pubs.acs.org/10.1021/acsapm.3c00861

### Author Contributions

The manuscript was written through contributions of all authors. All authors have given approval to the final version of the manuscript.

### Notes

The authors declare no competing financial interest.

## ■ ACKNOWLEDGMENTS

We thank David Dupret for the stainless steel microscrews used in the experiments and for suggestions for the manuscript and the project in the context of neural electrodes.

## ■ REFERENCES

(1) Aqrawe, Z.; Montgomery, J.; Travas-Sejdic, J.; Svirskis, D. Conducting Polymers as Electrode Coatings for Neuronal Multi-electrode Arrays. *Trends Biotechnol.* **2017**, *35*, 93−95.

(2) Charkhkar, H.; Knaack, G. L.; McHail, D. G.; Mandal, H. S.; Peixoto, N.; Rubinson, J. F.; Dumas, T. C.; Pancrazio, J. J. Chronic intracortical neural recordings using microelectrode arrays coated with PEDOT−TFB. *Acta Biomater.* **2016**, *32*, 57−67.

(3) Asplund, M.; Nyberg, T.; Inganäs, O. Electroactive polymers for neural interfaces. *Polym. Chem.* **2010**, *1*, 1374−1391.

(4) Yamato, H.; Ohwa, M.; Wernet, W. Stability of polypyrrole and poly(3,4-ethylenedioxythiophene) for biosensor application. *J. Electroanal. Chem.* **1995**, *397*, 163−170.

(5) Cui, X. T.; Zhou, D. D. Poly (3,4-ethylenedioxythiophene) for chronic neural stimulation. *IEEE Trans. Neural Syst. Rehabil. Eng.* **2007**, *15*, 502−508.

(6) Baek, S.; Green, R. A.; Poole-Warren, L. A. The biological and electrical trade-offs related to the thickness of conducting polymers for neural applications. *Acta Biomater.* **2014**, *10*, 3048−3058.

(7) Luo, S.-C.; Mohamed Ali, E.; Tansil, N. C.; Yu, H.-h.; Gao, S.; Kantchev, E. A. B.; Ying, J. Y. Poly(3,4-ethylenedioxythiophene) (PEDOT) Nanobiointerfaces: Thin, Ultrasmooth, and Functionalized PEDOT Films with in Vitro and in Vivo Biocompatibility. *Langmuir* **2008**, *24*, 8071−8077.

(8) Dijk, G.; Ruigrok, H. J.; O'Connor, R. P. Influence of PEDOT:PSS Coating Thickness on the Performance of Stimulation Electrodes. *Adv. Mater. Interfac.* **2020**, *7*, 2000675.

(9) Cui, X. Y.; Martin, D. C. Electrochemical deposition and characterization of poly(3,4-ethylenedioxythiophene) on neural microelectrode arrays. *Sens. Actuators, B* **2003**, *89*, 92−102.

(10) Ludwig, K. A.; Uram, J. D.; Yang, J. Y.; Martin, D. C.; Kipke, D. R. Chronic neural recordings using silicon microelectrode arrays electrochemically deposited with a poly(3,4-ethylenedioxythiophene) (PEDOT) film. *J. Neural. Eng.* **2006**, *3*, 59−70.

(11) Baek, S.; Green, R. A.; Poole-Warren, L. A. Effects of dopants on the biomechanical properties of conducting polymer films on platinum electrodes. *J. Biomed. Mater. Res., Part A* **2014**, *102*, 2743−2754.

(12) Bodart, C.; Rossetti, N.; Hagler, J.; Chevreau, P.; Chhin, D.; Soavi, F.; Schougaard, S. B.; Amzica, F.; Cicoira, F. Electropolymerized Poly(3,4-ethylenedioxythiophene) (PEDOT) Coatings for Implantable Deep-Brain-Stimulating Microelectrodes. *ACS Appl. Mater. Interfaces* **2019**, *11*, 17226−17233.

(13) Volkov, A. V.; Wijeratne, K.; Mitraka, E.; Ail, U.; Zhao, D.; Tybrandt, K.; Andreasen, J. W.; Berggren, M.; Crispin, X.; Zozoulenko, I. V. Understanding the Capacitance of PEDOT:PSS. *Adv. Funct. Mater.* **2017**, *27*, 1700329.

(14) Tamburri, E.; Orlanducci, S.; Toschi, F.; Terranova, M. L.; Passeri, D. Growth mechanisms, morphology, and electroactivity of PEDOT layers produced by electrochemical routes in aqueous medium. *Synth. Met.* **2009**, *159*, 406−414.

(15) Du, X.; Wang, Z. Effects of polymerization potential on the properties of electrosynthesized PEDOT films. *Electrochim. Acta* **2003**, *48*, 1713−1717.

(16) Kamensky, M. A.; Eliseeva, S. N.; Láng, G.; Ujvári, M.; Kondratiev, V. V. Electrochemical Properties of Overoxidized Poly-3,4-Ethylenedioxythiophene. *Russ. J. Electrochem.* **2018**, *54*, 893−901.

(17) Wang, D.; Pillier, F.; Cachet, H.; Debiemme-Chouvy, C. One-pot electrosynthesis of ultrathin overoxidized poly(3,4-ethylenedioxythiophene) films. *Electrochim. Acta* **2022**, *401*, 139472.

(18) Rivnay, J.; Owens, R. M.; Malliaras, G. G. The Rise of Organic Bioelectronics. *Chem. Mater.* **2014**, *26*, 679−685.

(19) Rivnay, J.; Leleux, P.; Ferro, M.; Sessolo, M.; Williamson, A.; Koutsouras, D. A.; Khodagholy, D.; Ramuz, M.; Strakosas, X.; Owens, R. M.; Benar, C.; Badier, J. M.; Bernard, C.; Malliaras, G. G. High-performance transistors for bioelectronics through tuning of channel thickness. *Sci. Adv.* **2015**, *1*, No. e1400251.

(20) Castagnola, V.; Bayon, C.; Descamps, E.; Bergaud, C. Morphology and conductivity of PEDOT layers produced by different electrochemical routes. *Synth. Met.* **2014**, *189*, 7−16.

(21) Rossetti, N.; Hagler, J.; Kateb, P.; Cicoira, F. Neural and electromyography PEDOT electrodes for invasive stimulation and recording. *J. Mater. Chem. C* **2021**, *9*, 7243−7263.

(22) Green, R. A.; Hassarati, R. T.; Bouchinet, L.; Lee, C. S.; Cheong, G. L. M.; Yu, J. F.; Dodds, C. W.; Suaning, G. J.; Poole-Warren, L. A.; Lovell, N. H. Substrate dependent stability of conducting polymer coatings on medical electrodes. *Biomaterials* **2012**, *33*, 5875−5886.

(23) Zeng, Q.; Wu, T. Z. Enhanced electrochemical performance of neural electrodes based on PEDOT:PSS hydrogel. *J. Appl. Polym. Sci.* **2022**, *139*, 51804.

(24) Hong, G. S.; Lieber, C. M. Author Correction: Novel electrode technologies for neural recordings. *Nat. Rev. Neurosci.* **2019**, *20*, 376.

(25) Boehler, C.; Carli, S.; Fadiga, L.; Stieglitz, T.; Asplund, M. Tutorial: guidelines for standardized performance tests for electrodes intended for neural interfaces and bioelectronics. *Nat. Protoc.* **2020**, *15*, 3557−3578.

(26) Bobacka, J.; Lewenstam, A.; Ivaska, A. Electrochemical impedance spectroscopy of oxidized poly(3,4-ethylenedioxythiophene) film electrodes in aqueous solutions. *J. Electroanal. Chem.* **2000**, *489*, 17−27.

(27) Carli, S.; Bianchi, M.; Zucchini, E.; Di Lauro, M.; Prato, M.; Murgia, M.; Fadiga, L.; Biscarini, F. Electrodeposited PEDOT:Nafion Composite for Neural Recording and Stimulation. *Adv. Healthcare Mater.* **2019**, *8*, 1900765.

(28) Yang, J.; Kim, D. H.; Hendricks, J. L.; Leach, M.; Northey, R.; Martin, D. C. Ordered surfactant-templated poly(3,4-ethylenedioxythiophene) (PEDOT) conducting polymer on microfabricated neural probes. *Acta Biomater.* **2005**, *1*, 125−136.

(29) Luo, X.; Weaver, C. L.; Zhou, D. D.; Greenberg, R.; Cui, X. T. Highly stable carbon nanotube doped poly(3,4-ethylenedioxythiophene) for chronic neural stimulation. *Biomaterials* **2011**, *32*, 5551−5557.

(30) Alba, N. A.; Du, Z. J.; Catt, K. A.; Kozai, T. D.; Cui, X. T. In Vivo Electrochemical Analysis of a PEDOT/MWCNT Neural Electrode Coating. *Biosensors* **2015**, *5*, 618−646.
(31) Sader, J. E.; Borgani, R.; Gibson, C. T.; Haviland, D. B.; Higgins, M. J.; Kilpatrick, J. I.; Lu, J.; Mulvaney, P.; Shearer, C. J.; Slattery, A. D.; Thoren, P. A.; Tran, J.; Zhang, H.; Zhang, H.; Zheng, T. A virtual instrument to standardise the calibration of atomic force microscope cantilevers. *Rev. Sci. Instrum.* **2016**, *87*, 093711.
(32) Voïtchovsky, K.; Kuna, J. J.; Contera, S. A.; Tosatti, E.; Stellacci, F. Direct mapping of the solid−liquid adhesion energy with subnanometre resolution. *Nat. Nanotechnol.* **2010**, *5*, 401−405.
(33) Igor Pro Manual Version 9. 2017, https://www.wavemetrics.net/doc/IgorMan.pdf (accessed May 25, 2023).
(34) Contera, S. A.; Voïtchovsky, K.; Ryan, J. F. Controlled ionic condensation at the surface of a native extremophilemembrane. *Nanoscale* **2010**, *2*, 222−229.
(35) Wang, Y.; Song, R.; Li, Y.; Shen, J. Understanding tapping-mode atomic force microscopy data on the surface of soft block copolymers. *Surf. Sci.* **2003**, *530*, 136−148.
(36) Modarresi, M.; Mehandzhiyski, A.; Fahlman, M.; Tybrandt, K.; Zozoulenko, I. Microscopic Understanding of the Granular Structure and the Swelling of PEDOT:PSS. *Macromolecules* **2020**, *53*, 6267−6278.
(37) Xia, Z.; Arias-Gil, G.; Deckert, M.; Vollmer, M.; Curran, A.; Herrera-Molina, R.; Brosch, M.; Krug, K.; Schmidt, B.; Ohl, F. W.; Lippert, M. T.; Takagaki, K. Electrochemical Roughening and Carbon Nanotube Coating of Tetrodes for Chronic Single-Unit Recording. bioRxiv. **2019**, 738245, 10.1101/738245.
(38) Marblestone, A. H.; Zamft, B. M.; Maguire, Y. G.; Shapiro, M. G.; Cybulski, T. R.; Glaser, J. I.; Amodei, D.; Stranges, P. B.; Kalhor, R.; Dalrymple, D. A.; Seo, D.; Alon, E.; Maharbiz, M. M.; Carmena, J. M.; Rabaey, J. M.; Boyden, E. S.; Church, G. M.; Kording, K. P. Physical principles for scalable neural recording. *Front. Comput. Neurosci.* **2013**, *7*, 137.
(39) van de Ven, G. M.; Trouche, S.; McNamara, C. G.; Allen, K.; Dupret, D. Hippocampal Offline Reactivation Consolidates Recently Formed Cell Assembly Patterns during Sharp Wave-Ripples. *Neuron* **2016**, *92*, 968−974.




https://doi.org/10.1021/acsapm.3c00861
*ACS Appl. Polym. Mater.* 2023, 5, 5555−5566